Journal of Colloid and Interface Science 345 (2010) 131–137

Contents lists available at ScienceDirect

Journal of Colloid and Interface Science

www.elsevier.com/locate/jcis

Monodisperse, high refractive index, highly charged ZnS colloids self assemble into crystalline colloidal arrays

Jia Luo, Dan Qu, Alexander Tikhonov, Justin Bohn, Sanford A. Asher *

Department of Chemistry, University of Pittsburgh, Pittsburgh, PA 15260, United States

ARTICLE INFO

Article history:
Received 3 June 2009
Accepted 3 February 2010
Available online 10 February 2010

Keywords:
Monodisperse
Surface charge
High refractive index
Photonic crystal

ABSTRACT

We developed an efficient synthesis of monodisperse, highly surface charged, high refractive index ZnS spherical particles by using a gel–sol method. Concentrated solutions of zinc–ammonia–NTA (nitrilotriacetic acid) were reacted with thioacetamide in the presence of gelatin which stabilized the growing particles. We dramatically increased the particle surface charge density by condensing silica and silylated phosphonate groups on the particle surface. These monodisperse highly charged ZnS particles are somewhat porous and have a refractive index of 1.868. These are the highest refractive index, monodisperse, highly charged spherical particles to self assemble into non-close-packed crystalline colloidal arrays which Bragg diffract light.

1. Introduction

Photonic crystals materials contain periodic modulations of their optical dielectric constants. As a result, these materials show optical bandgaps such that light in specific spectral regions cannot propagate at specific angles [1–4]. These bandgaps can be one or two dimensional, where light cannot propagate within particular angular ranges. In addition, these bandgaps can be three dimensional, such that light in a particular spectral interval cannot propagate at any angle within the photonic crystal. These materials are of great interest both for fundamental scientific reasons, as well as, for their potential for revolutionizing photonic technologies [5–11].

Photonic crystal materials can be fabricated by either using top-down lithographic approaches [12,13], or by using bottom-up approaches such as colloidal crystal self assembly techniques [14–20]. The use of top-down lithography [12,13] is generally expensive and its use is limited to fabricating a finite number of periodic layers. Bottom-up approaches have the opportunity to be inexpensive and to be easily scaled up. Examples of bottom-up fabrication processes of photonic crystals include production of close-packed particle arrays through techniques [14–20] such as, for example, gravity or external field driven sedimentation [14,15] or convective self assembly [16].

A potential disadvantage of sedimentation processes is that the resulting close-packed materials typically contain numerous defects such as vacancies, dislocations, stacking faults, and grain boundaries [21]. The convective self assembly method can give rise to better ordered close-packed systems but the success of this method is sensitive to particle size and charge [22]. In addition, it is unclear whether this method can be easily scaled up to produce large area, thick photonic crystals.

Electrostatic self assembly of highly charged, monodisperse colloids is an alternative approach which appears much more convenient since the particles directly self assemble into highly ordered fcc or bcc crystalline colloidal arrays (CCA) in low ionic strength, aqueous solutions [23–25]. This self assembly occurs within the entire colloid dispersion volume. The only question is whether crystal orientation can be maintained over large sample thicknesses, since crystal nucleation often occurs at the walls of the container [26]. These CCA diffract ultra-violet, visible, or infra-red light, depending on their crystal lattice spacing [27,28].

Although the diffraction properties of CCA have been extensively studied, these studies have generally been limited to colloidal particles of low refractive index materials [23,24,29–36]. The production of full three dimensional bandgaps in photonic crystals requires specific crystal structures together with very high modulations of their optical dielectric constants. For an inverted fcc lattice (air sphere in high dielectric medium), a full photonic band gap will open up between the 8th and 9th bands if the refractive index mismatch exceeds 2.9 [37]. Close-packed inverse opal structures of air spheres in silicon [38] and germanium [39] have been fabricated which show complete photonic band gaps in the NIR region.

Unfortunately, no complete 3-D photonic band gap occurs for dielectric spheres in direct fcc structures [40,41]. The diffraction efficiency of all photonic crystals is generally increased by increasing the refractive index mismatch between the spheres and the

* Corresponding author. Fax: +1 412 624 0588.
E-mail address: asher@pitt.edu (S.A. Asher).

0021-9797/$ - see front matter © 2010 Elsevier Inc. All rights reserved.
doi:10.1016/j.jcis.2010.02.002

medium [23]. A number of groups have synthesized high refractive index monodisperse spheres out of semiconductor materials such as ZnS, Se, CdSe and TiO_2 in order to prepare high refractive index modulated photonic crystal materials [42–47]. However, the use of these spheres has been limited to close-packed photonic crystal systems.

In the work here we demonstrate the synthesis of novel high refractive index, monodisperse, highly surface charged ZnS particles that are surface functionalized such that they form non-close-packed electrostatically stabilized CCA. We use a method similar to that of Sugimoto et al. [48,49] to synthesize the monodisperse ZnS particles from concentrated solutions of zinc–chelate complexes in gelatin which effectively prevents growing particles from aggregating [50] at the required high ionic strength conditions. We can easily control the particle size and the size distribution. We maximized the ZnS surface charge density by simultaneously condensing silica and functionalizing the particles with a phosphonate silane coupling agent. The highly charged, monodisperse ZnS colloids self-assemble into CCA at high concentrations and low ionic strengths. These CCA with $\varepsilon = 3.49$ ($n = 1.87$) particles diffract light in the near IR and the visible regions.

2. Experimental section

2.1. Chemicals

Zinc nitrate hexahydrate $Zn(NO_3)_2{\cdot}6H_2O$ (purum p.a. >99.0%) was purchased from Fluka (Germany). Ammonium acetate (ACS reagent 98%), ammonia (ACS grade, 28–30 wt.% NH_3 in water) and absolute ethanol were obtained from Mallinckrodt Baker Inc. (Phillipsburg, NJ). Nitrilotriacetic acid (NTA) (Sigma grade 99%), thioacetamide (TAA, reagent grade 98%), porcine skin gelatin (type A, 300 bloom), gelatin from cold water fish skin and tetraethoxysilane (TEOS, 99%) were obtained from Sigma–Aldrich (St. Louis, MO). 3-trihydroxylsilylpropylmethylphosphonate, sodium salt, 42% in water was purchased from Gelest Inc. Ion exchange resin (AG 501-X8, 20–50 mesh) was obtained from Bio-Rad Laboratories Inc. All chemicals were used as received without further purification. Pure water was obtained from a Barnstead nano-pure water system.

2.2. Preparation of monodisperse ZnS particles

ZnS particles were synthesized by using a method similar to the gel–sol process described by Sugimoto et al. [49]. ZnS particles were formed by mixing thioacetamide (TAA) solution with a concentrated solution of zinc–nitrilotriacetate (Zn–NTA). In one recipe, the thioacetamide (TAA) solution was prepared by dissolving 1.38 g (0.018 mol) TAA and 0.15 g (1% by wt.) porcine skin gelatin (type A, 300 bloom) in 15 ml pure water. The Zn–NTA solution was prepared by dissolving 5.36 g (0.018 mol) $Zn(NO_3)_2{\cdot}6H_2O$, 9.25 g (0.12 mol) CH_3COONH_4, 6.88 g (0.036 mol) NTA, 12 ml ammonia (28–30 wt.% NH_3 in water) and 0.60 g (1% by wt.) porcine skin gelatin (type A, 300 bloom) in pure water. The total volume was adjusted to 60 ml. The Zn–NTA solution at 45 °C was adjusted to pH ~ 9.0 by adding NH_4OH. To initiate ZnS nucleation, a 45 °C TAA solution was then poured into the 45 °C Zn–NTA solution under vigorous stirring. After 1 min the stirring was stopped and the reaction mixture was maintained at 45 °C for 4 h.

The ZnS nanoparticles were separated and purified by adding concentrated NaOH solution at 60 °C under vigorous stirring to hydrolyze the gelatin. The zinc sulfide particles were centrifuged, redispersed and washed multiple times with pure water. TEM of the resulting particles are shown in Fig. 1.

2.3. Attachment of ZnS particle surface charge

In a typical synthesis, 1.0 ml tetraethoxysilane (TEOS) and 1.0 ml of 3-trihydroxylsilylpropylmethylphosphonate aqueous solution (42 wt.%) were added to a 100 ml aqueous suspension containing 1.0 g ZnS colloids, 40 ml ethanol and 1.0 ml ammonium hydroxide, and the reaction mixture was heated to 80 °C and remained under reflux for 4 h. For a control we used the same reaction conditions but did not add the phosphonate silane coupling agent but only added TEOS.

2.4. Materials characterization

X-ray diffraction measurements were carried out by utilizing a Philips PW 3710 based X'per diffractometer systems using Cu Kα radiation from a Philips PW 1830 X-ray generator. A Philips Mogagni 268 transmission electron microscope was used to characterize the size of the particles synthesized. A Zeta PALS QELS instrument (Brookhaven Instruments Corporation) was used to measure the Zeta potential of the colloidal particles. All the Zeta potential measurements were taken by suspending a small amount of colloidal particles in a 1 mM KCl solution. The pH of the suspensions was varied from 3 to 12 using dilute HCl and NaOH solutions. A YSI 3200 conductivity instrument was used to measure the conductance of the colloidal suspensions.

A Craic QDI 2010 UV–Visible–NIR microspectrophotometer was used to measure some of the normal incidence reflectance spectra

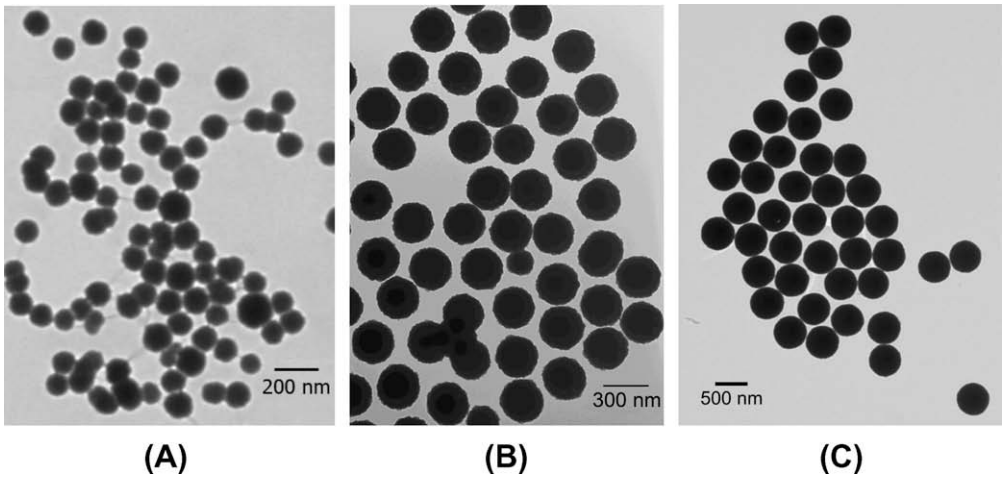

Fig. 1. Transmission electron microscope images of zinc sulfide particles after washing (A) 125 ± 13 nm; (B) 285 ± 9 nm; (C) 498 ± 18 nm.

of the ZnS particle CCA. Normal incidence reflectance measurements were also made by using a fiber-optic diode spectrometer with a tungsten halogen light source (Ocean Optics). A Varian Cary 5000 UV–Visible spectrometer was used to measure transmission spectra of thin CCA films. Variable angle reflectance (VAR) spectra of the ZnS CCA were measured by using the VAR accessory of a Varian Cary 5000 spectrophotometer.

3. Results and discussions

3.1. Synthesis and characterization of zinc sulfide particles

Monodisperse ZnS particles between 100 and 600 nm were produced by varying the reaction stoichiometry. TEM images of some typical monodisperse zinc sulfide particle samples are shown in Fig. 1.

The X-ray diffraction pattern shown in Fig. 2 from the prepared ZnS particles indicates that the particles synthesized are in the ZnS cubic sphalerite phase.

The Zeta potentials of the synthesized ~500 nm ZnS particles were measured to be −4 mV ± 25 mV at pH 7. The pure ZnS particle suspensions appear white and do not show any trace of CCA ordering that would give rise to visible wavelength light diffraction even for particle concentrations above 10% by volume. Presumably, no ordered CCA formed because of insufficient ZnS particle surface charge.

The synthesis of the monodisperse ZnS particles involves two steps: a fast nucleation step and a slow growth step. In basic media, the reaction involves the reaction of a concentrated Zn–NTA solution with TAA.

$$CH_3{-}CS{-}NH_2(aq) \leftrightarrow CH_3CN(aq) + H_2S(aq)$$
$$H_2S(aq) + H_2O \rightarrow HS^-(aq) + H_2O \rightarrow S^{2-}(aq) + H_3O^+$$
$$Zn^{2+}(aq) + S^{2-}(aq) \rightarrow ZnS(s)$$

According to Sugimoto [48], if the H_2S concentration is too high, addition of concentrated Zn^{2+} solutions results in random agglomeration which forms a large number of nuclei. To avoid this, chelating agents are used that coordinate to the Zn^{2+}, reducing its free concentration. Zn^{2+} is slowly released to react with S^{2-} to form a presumably soluble, small ZnS "precursor" species [51]. ZnS particle nuclei form when the concentration of dissolved ZnS "precursor" exceeds the critical supersaturation concentration. Nuclei continue to form until the ZnS "precursor" concentration drops below the critical supersaturation level. These nuclei will grow homogeneously to form monodisperse ZnS particles if secondary nucleation is prevented.

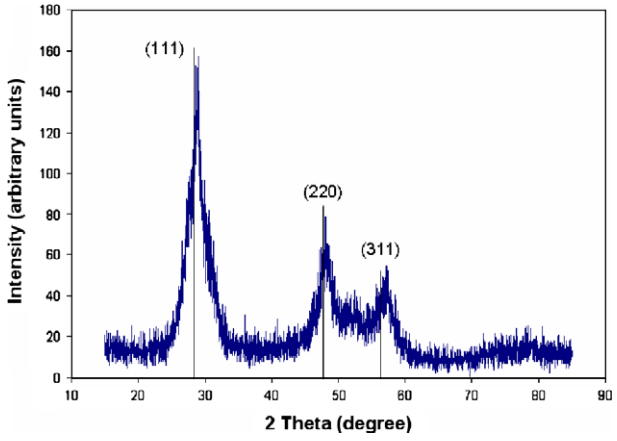

Fig. 2. X-ray powder diffraction pattern of synthesized ZnS particles. The indexing indicates the cubic sphalerite phase (Powder Diffraction File card number 80-0020).

Table 1 tabulates the impact of compositional changes on the final particle size. Four parameters, the initial $[Zn(NO_3)_2]$, the [NTA]/[Zn], the $[NH_3 + NH_4^+]$ and the pH values were varied to control the final particle size. The pH values were varied by adding ammonia to the Zn–NTA solution containing 1.6 M CH_3COONH_4. Table 1A shows that the particle size decreases as the amount of ammonia increases, while $[Zn(NO_3)_2]$ and [NTA]/[Zn] are held constant (the pH increases as the ammonia concentration increases). Table 1B shows that particle size decreases when [NTA]/[Zn] and $[NH_3 + NH_4^+]$ simultaneously decrease, while $[Zn(NO_3)_2]$ is held constant and the relative amounts of NTA to ammonia is varied to maintain pH = 9.0. Table 1C shows that particle size increases when the concentration of $Zn(NO_3)_2$ decreases, while [NTA]/[Zn] is held constant. The $[NH_3 + NH_4^+]$ is varied to maintain pH = 9.0.

To obtain monodisperse particles we find that stirring must be stopped shortly after mixing the reactants. In our case, stirring throughout the reaction results in a larger polydispersity which might arise from secondary nucleation. As pointed out by Sugimoto et al. [49], agitation may release subcrystals from the polycrystalline ZnS particles which can result in secondary nucleation during the particle growth period.

Gelatin was added to the reaction solution to prevent growing ZnS particles from aggregating under our high ionic strength conditions [52]. Without gelatin, ZnS particles aggregate and settle shortly after the nucleation stage.

We find that the polydispersity of our synthesized particles depends on the gelatin type and the reaction temperature. For example, for a particular reaction stoichiometry using porcine skin gelatin the particles are monodisperse (PD = 5%) if the reaction occurs at 60 °C. The particles become polydisperse (PD = 16%) for reaction temperatures below 40 °C. The porcine skin gelatin shows a helix to coil conformational transition at 40 °C. The transition temperature varies between different gelatins [53]. For example, gelatin made from cold water fish skin has a transition temperature of 22 °C [54]. Using gelatin from cold water fish skin we can obtain monodisperse particles at room temperature (~22 °C, PD = 6%), as well as at 30 °C, (PD = 4%).

Thus, it appears that the gelatin coil conformation increases the particle monodispersity. The improved monodispersity of reactions above the gelatin transition temperature results from the adsorption of gelatin layers as random coils on the particle surface which protect the particles from aggregation [55–57].

Table 1
Relationship between the size of monodisperse ZnS particles and the solution stoichiometry. (Reaction temperature was 45 °C and the yields for all the samples are ~90%. TEM images of samples marked with asterisks are shown in Fig. 1.).

A. $[Zn(NO_3)_2]$ = 0.28 M, [NTA]/[Zn] = 1.8		
$[NH_3 + NH_4^+]$ (M)	pH	Size (nm)
3.7	9.0	150 ± 30
4.0	9.4	125 ± 13*
4.4	9.6	120 ± 12
4.8	9.9	105 ± 18
B. $[Zn(NO_3)_2]$ = 0.24 M, pH = 9.0		
$[NH_3 + NH_4^+]$ (M)	[NTA]/[Zn]	Size (nm)
4.0	2.2	323 ± 19
3.75	2.0	285 ± 9*
3.0	1.8	238 ± 20
2.9	1.7	225 ± 19
C. [NTA]/[Zn] = 2.0, pH = 9.0		
$[NH_3 + NH_4^+]$ (M)	$[Zn(NO_3)_2]$ (M)	Size (nm)
4.35	0.28	146 ± 33
3.75	0.24	285 ± 9*
2.8	0.18	498 ± 18*

3.2. Functionalization of ZnS particle surfaces

The ZnS particle diameter increases relatively little after reaction with TEOS and the phosphonate silane coupling agent compared to the particle diameter standard deviation. For example, the diameter of the 498 ± 18 nm and 458 ± 18 nm bare ZnS particles increased to 506 ± 17 nm and 472 ± 12 nm respectively, after simultaneously reacting with TEOS and the phosphonate silane coupling agent. The reaction is obviously incomplete since we expect to observe an 80 nm and 72 nm diameter increase respectively, if all of the TEOS and the phosphonate silane coupling agent condensed onto the particle surface. Consistent with this observation is that we see significant formation of small particles in the TEM of the ZnS particles reacted with TEOS and the phosphonate silane coupling agent (Fig. 3A, 472 ± 12 nm sample). The concentration of small particles is roughly comparable to that which occurs after TEOS and phosphonate silane are reacted in the absence of ZnS under the same condition (Fig. 3C). These small particles can be removed by centrifuging and washing (Fig. 3B). As seen below, the surface charge is increased by this TEOS and phosphonate silane coupling agent reaction which forms a very thin nonobservable shell.

Fig. 4 shows the pH dependence of the Zeta potential of the ~500 nm ZnS particles before, and after simultaneous reaction with TEOS and the phosphonate silane coupling agent in order to increase surface charge. Also shown is the pH dependence of the Zeta potential of the product of the reaction of the ZnS particles with only TEOS. The bare ZnS particles are almost uncharged at neutral pH. The absolute magnitude of the charge increases (and the sign inverts) as the pH increases or decreases away from neutrality, presumably due to ion adsorption onto the particles.

ZnS particles reacted with only TEOS have a much higher Zeta potential at all pH values than the bare ZnS particles. The TEOS reacted particle surface groups titrate over a broad pH range with a $pK_a \sim 6$, within the range of pK_a discussed for silica surfaces [58–60]. ZnS particles simultaneously reacted with TEOS and the phosphonate silane coupling agent (ZnSTP) show a distinctly higher Zeta potential until pH > 9. The apparent $pK_a \sim 3$, which gives rise to a distinctly higher Zeta potential, indicates a higher surface charge at acidic and neutral pH values due to deprotonation of the attached phosphonate group. The pK_a of propyl methylphosphonic acid is 2.29 [61].

3.3. Formation of ZnS crystalline colloidal arrays

When the monodisperse ZnSTP colloidal particles are concentrated to 8–10 vol.%, they self assemble due to Coulombic repulsive interactions into CCA [25,28] which diffract light at a wavelength that depends on the CCA lattice spacing [24,62].

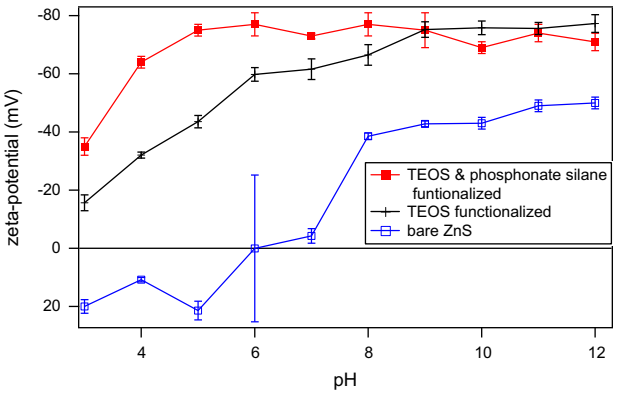

Fig. 4. Zeta potential vs. pH for bare ZnS particles, particles functionalized by only TEOS, and particles functionalized with TEOS and phosphonate silane coupling agent (ZnSTP). Bare ZnS particle diameter is 498 ± 18 nm. The large Zeta potential variation at pH 7 for bare ZnS particle presumably results from aggregation at low particle charge.

Fig. 5 shows transmission spectra of the 498 nm bare ZnS particles, the ZnS particles reacted with only TEOS and the 506 nm ZnSTP particles injected into 50 μm thick flow cells. The colloid suspensions were repeatedly pumped back and forth in the flow cell to achieve shear ordering. The cell was then tapped to induce mechanical perturbations that cause CCA annealing. All spectra were referenced to the transmission spectra of the same flow cell containing water.

The lack of a transmission minimum and the monotonic transmission decrease towards shorter wavelength indicate that the bare ZnS particles do not form CCA (due to their low surface charge). The transmission decreases as the wavelength decreases due to the increasing scattering cross section of these particles at shorter wavelength. This bare ZnS particle sample also showed visually evident particle flocculation.

Particles reacted with TEOS form a CCA with a broad, essentially complete rejection band at 1720 nm. The diffraction band is broad and asymmetric. Normally, fcc (sometimes bcc) CCA form with their (1 1 1) planes aligned parallel to the sample walls. A perfect fcc crystal illuminated by light normally incident to the (1 1 1) planes will diffract the longest wavelength light, λ_{111}, from the (1 1 1) planes as given by Bragg's Law, $\lambda_{111} = 2nd_{111}$, where n is the system refractive index and d_{111} is the (1 1 1) plane spacing.

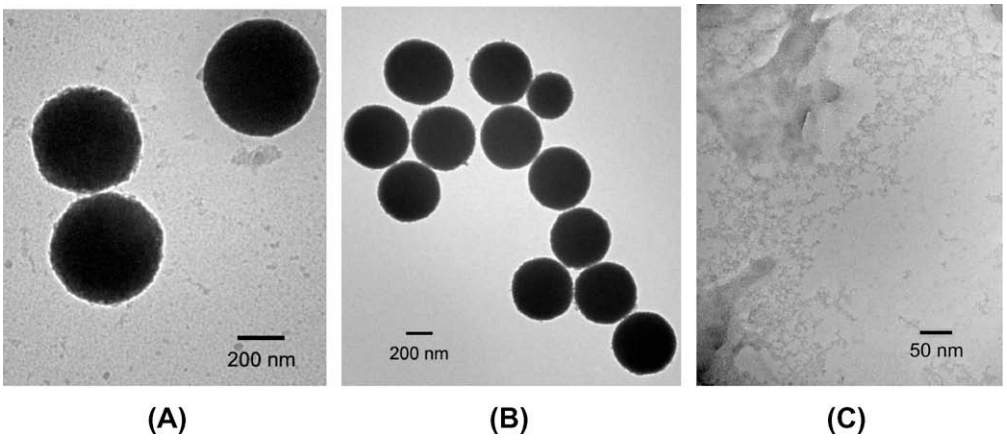

Fig. 3. TEM of (A) 472 ± 12 nm ZnSTP colloids suspension after simultaneous reaction with TEOS and the phosphonate silane coupling agent directly out from the reaction mixture; (B) 472 ± 12 nm ZnSTP particles after washing to remove the small particles; (C) the reaction mixture after TEOS and phosphonate silane coupling agent are reacted in the absence of ZnS particles under the same conditions.

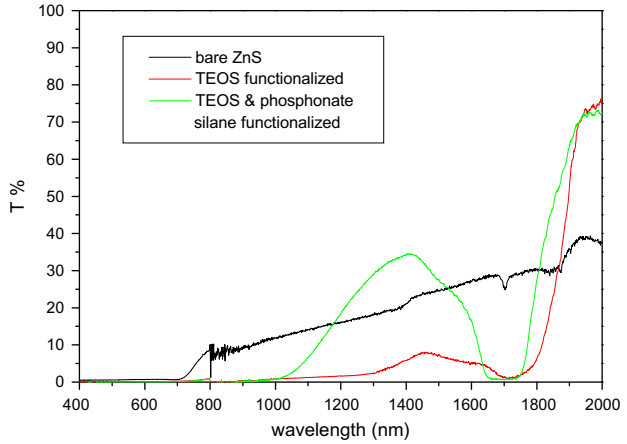

Fig. 5. Transmission spectra taken in a 50 μm thick flow cell of bare ZnS, ZnS functionalized with TEOS, and ZnS functionalized with TEOS and phosphonate silane (ZnSTP). All of these samples were extensively washed and ion exchanged.

For light at normal incidence no diffraction should be observed for shorter wavelengths until $\lambda_{111}/2$. The observed low transmission at wavelengths between 1000 and 1600 nm indicates that the ZnS particles reacted only with TEOS shows poor ordering.

Ordering is much improved for the ZnSTP particles simultaneously reacted with TEOS and the phosphonate silane coupling agent (Fig. 5). The 1700 nm diffraction peak is much better defined and less scattering occurs in the 1000–1600 nm spectral region. This clearly indicates that ZnSTP particles reacted with TEOS and phosphonate silane coupling agent have the highest surface charge (as also evidenced by the Zeta potential results).

Reflectance spectra of the CCA formed from ZnSTP are shown in Fig. 6. Diffraction from the (1 1 1) planes gives rise to the 1708 nm reflection diffraction peak. To determine the refractive index of the ZnSTP particles we measured variable angle reflectance spectra of the ZnSTP CCA (Fig. 6 inset). The 1st order (1 1 1) diffraction peaks blue shift as the incident angle changes from 20° to 29°, respectively.

To determine the light incidence angle dependence of the diffraction we must account for refraction of the incident light from Snell's law:

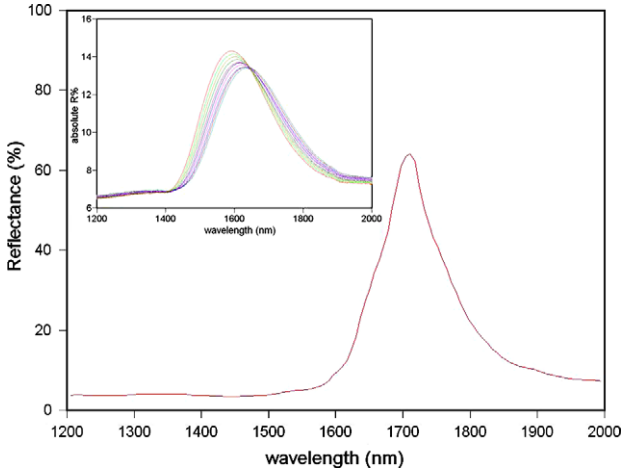

Fig. 6. Reflectance spectra of a CCA sample of 506 nm ZnSTP particles in a 700 μm thick flow cell measured with a Craic microspectrophotometer. The (1 1 1) peak position at normal incidence is 1708 nm. The inset shows the incident angle dependence of the fcc (1 1 1) reflectance spectra of the CCA sample from right to left from 20° to 29°, respectively.

$$\frac{\sin\theta_{\text{air}}}{\sin\theta_{\text{PhC}}} = n_{\text{PhC}} \tag{1}$$

Bragg's law thus gives:

$$\lambda_{111} = 2n_{\text{PhC}}d_{111}\sin(90^\circ - \theta_{\text{PhC}}) \tag{2}$$

where n_{PhC} is the overall effective refractive index of the ZnSTP CCA which we approximate as the volume averaged refractive index:

$$n_{\text{PhC}} = (1-\varphi)n_{\text{water}} + \varphi \cdot n_{\text{ZnSTP}} \tag{3}$$

where φ is the volume fraction occupied by the ZnSTP spheres.

The refractive indices of ZnS [63] and water are weakly wavelength dependent [64]:

$$n^2_{\text{ZnS}} = 5.164 + \frac{1.208\times10^5}{\lambda^2 - 0.732\times10^5} \tag{4}$$

$$n_{\text{water}} = 1.3240 + \frac{3.046\times10^3}{\lambda^2} \tag{5}$$

where the wavelength λ is in units of nm. In a small wavelength range, the refractive indices can be considered constant. Thus, from Eqs. (1) and (2), we have

$$\lambda^2_{111} = -4\cdot d^2_{111}\cdot\sin\theta^2_{\text{air}} + 4\cdot n^2_{\text{PhC}}\cdot d^2_{111} \tag{6}$$

From the reflectance spectra, we calculate a (1 1 1) lattice plane spacing of d_{111} = 580.0 nm with an average CCA refractive index of n_{PhC} = 1.468. The ZnSTP colloid particle diameter is 506 ± 17 nm from the TEM measurements, while the calculated volume fraction of ZnSTP colloid in the suspension is 0.268 ± 0.027, and the calculated weight fraction is 0.594 ± 0.0083, which agrees with our measured weight fraction of 0.612 ± 0.012. In this wavelength range, the water refractive index is $n_{\text{water}} \sim 1.325$, and we can calculate that the refractive index of the ZnSTP composite particle is 1.868 ± 0.007. Since bulk ZnS has a refractive index n = 2.283 at this wavelength, our ZnSTP particles must not be fully dense. This allows us to calculate a porosity which we assume is water filled of ~43%.

From the angle dependent diffraction measurements we calculate the normal incidence (1 1 1) diffraction peak to be at 1704 nm, which is close to the measured normal incidence (1 1 1) diffraction peak wavelength at 1708 nm measured in reflection with a Craic microspectrophotometer.

3.4. Ordering of ZnSTP CCA

Fig. 7 compares the diffraction from CCA of the 506 nm ZnSTP particles as a function of sample ordering. All of the CCA show a small transmission even at the ~1660 nm transmission minimum. The green spectrum from the ZnSTP sample simply injected with a minimum shear flow alignment is the broadest, showing a minimum transmission globally. The blue spectrum from the sample subject to shear by pumping the CCA back and forth in the flow cell is narrower and shows more transmission at shorter wavelengths. The black spectrum is the best ordered CCA because it was subject to both shear and mechanical tapping to induce maximum CCA ordering. It has the narrowest transmission peak and the most transmission at shorter wavelengths. The inset to Fig. 7 shows the reflection spectrum between 500 and 1000 nm and demonstrates strong second order diffraction at almost half of the 1660 nm transmission minimum of the most ordered sample.

Fig. 7 also shows the theoretical transmission spectrum due to diffraction by a perfect fcc CCA of 506 nm ZnSTP particles at the same concentration. We recently developed an extended kinematic theory for calculating the diffraction of perfect fcc CCA [65]. We calculated the diffraction expected for a CCA of 20 fcc (1 1 1) layers (11 μm) and 80 fcc (1 1 1) layers (44 μm) compared to the 50 μm

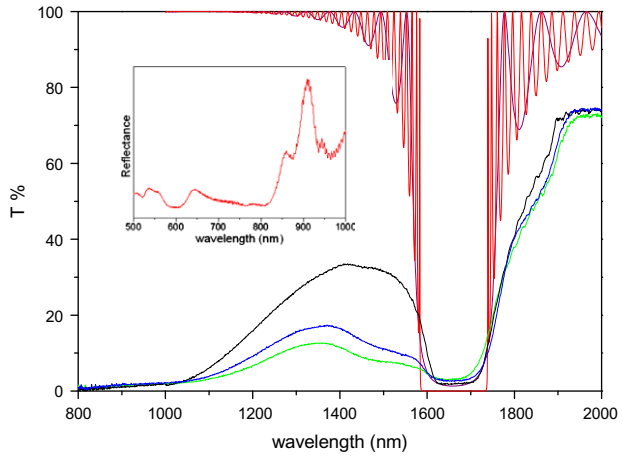

Fig. 7. Transmission spectra of a CCA sample of 506 nm ZnSTP particles in a 50 μm thick flow cell. The spectra are taken right after injection of the CCA (green); after shear flow (blue); after tapping and annealing (black). The transmission dip at ~1660 nm results from 1st order Bragg diffractions from the (1 1 1) planes. The (1 1 1) lattice spacing is calculated to be 555 nm, indicating a sample thickness of 90 layers. Theoretical transmission calculations for perfect fcc lattice of 506 nm particles of $n = 1.868$ in water (burgundy 20 layers, red 80 layers). Inset shows the normal incidence reflectance in the second order diffraction region of the same sample (For interpretation of the references to colour in this figure legend, the reader is referred to the web version of this article.).

thick ZnSTP sample. We calculate that 20 layers should transmit ~2% of the light, whereas 80 layers will transmit only 5×10^{-8}% of the light. The fact that 2% of the light transmits through our 90 layer sample indicates that CCA disorder degrades the diffraction compared to the perfect lattice.

Fig. 8 compares the transmission spectrum of a very thin CCA (~3.94 μm) of these 506 nm ZnSTP particles which was made by sandwiching 10 μL of the ZnSTP particle suspension between two quartz plates. The CCA thickness was determined from the observed interference fringes [66]. The transmission spectra were referenced to the transmission spectrum of the same two quartz plates containing water with approximately the same thickness. From Bragg's law, the (1 1 1) lattice spacing was calculated to be about 494 nm, indicating that the ~8 CCA (1 1 1) layers diffract

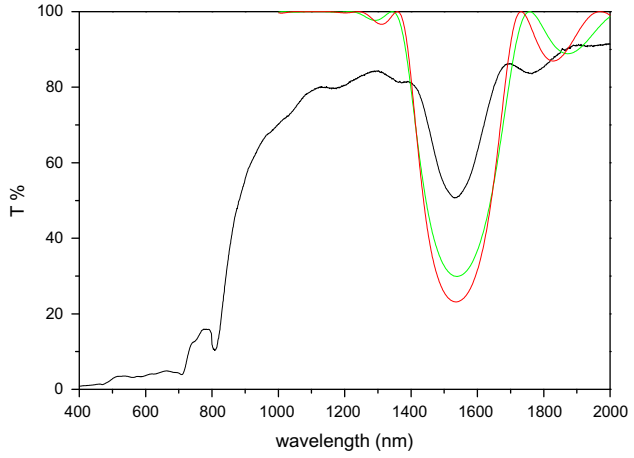

Fig. 8. Transmission spectrum for normally incident light of a ~3.94 μm thick CCA sample of 506 nm ZnSTP particles (~8 fcc (1 1 1) layers). The transmission minimum at 1542 nm results from the 1st order Bragg diffraction from the (1 1 1) planes. The green and red curves indicate the theoretically expected diffraction from perfect fcc lattice of 506 nm ZnSTP particles in water of eight and nine layers respectively (For interpretation of the references to colour in this figure legend, the reader is referred to the web version of this article.).

~50% of the light. Our theoretical calculation for a perfect lattice indicates that the diffraction should be ~2-fold greater.

4. Conclusions

We successfully fabricated high refractive index particle crystalline colloidal arrays (CCA) by synthesizing highly charged, monodisperse, high refractive index ZnS particles in the size range of 100–600 nm. The high surface charge density was obtained by simultaneously condensing silica and a silylated phosphonate group onto the particle surface. The resulting highly charged ZnS particles readily self-assemble into CCA. The refractive index of these ZnS particles was measured to be 1.868. The CCA sample shows high attenuation of light at wavelengths that coincide with 1st order (1 1 1) Bragg diffraction. These high refractive index particles should find utility in highly efficiency photonic crystal materials.

Acknowledgments

We acknowledge the support of this work by PPG Grant No. 218363 and NSF Grant: CHE-0848265.

References

[1] E. Yablonovitch, Phys. Rev. Lett. 58 (20) (1987) 2059–2062.
[2] S. John, Phys. Rev. Lett. 58 (23) (1987) 2486–2489.
[3] J.D. Joannopoulos, Robert D. Meade, Joshua N. Winn, Photonic Crystals: Moulding the Flow of Light, first ed., Princeton University Press, New York, 1995.
[4] C. Kittel, Introduction to Solid State Physics, eight ed., John Wiley and Sons Inc., Hoboken, NJ, 2005.
[5] M. Notomi, Phys. Rev. B: Condens. Matter Mater. Phys. 62 (16) (2000) 10696–10705.
[6] H. Miguez, V. Kitaev, G.A. Ozin, Appl. Phys. Lett. 84 (8) (2004) 1239–1241.
[7] S. John, Q. Tran, Phys. Rev. Lett. 78 (10) (1997) 1888–1891.
[8] P. Russell, Science (Washington, DC, U. S.) 299 (5605) (2003) 358–362.
[9] R.D. Meade et al., J. Appl. Phys. 75 (9) (1994) 4753–4755.
[10] A. Mekis et al., Phys. Rev. Lett. 77 (18) (1996) 3787–3790.
[11] A. Mihi, F.J. Lopez-Alcaraz, H. Miguez, Appl. Phys. Lett. 88 (19) (2006) 193110/1–193110/3.
[12] N. Yamamoto, S. Noda, A. Chutinan, Jpn. J. Appl. Phys., Part 2 37 (12A) (1998) L1491.
[13] J.G. Fleming, S.-Y. Lin, Opt. Lett. 24 (1) (1999) 49–51.
[14] M. Trau, D.A. Saville, I.A. Aksay, Science (Washington, DC) 272 (5262) (1996) 706–709.
[15] M. Holgado et al., Langmuir 15 (14) (1999) 4701–4704.
[16] P. Jiang et al., Chem. Mater. 11 (8) (1999) 2132–2140.
[17] A.S. Dimitrov et al., Langmuir 10 (2) (1994) 432–440.
[18] S.H. Park, D. Qin, Y. Xia, Adv. Mater. (Weinheim, Ger.) 10 (13) (1998) 1028–1032.
[19] Y. Lu et al., Langmuir 17 (20) (2001) 6344–6350.
[20] A. Mihi, M. Ocana, H. Miguez, Adv. Mater. (Weinheim, Ger.) 18 (17) (2006) 2244–2249.
[21] Y.A. Vlasov et al., Phys. Rev. E: Stat. Phys., Plasmas, Fluids, Relat. Interdisciplinary Top. 61 (5-B) (2000) 5784–5793.
[22] S. Wong, V. Kitaev, G.A. Ozin, J. Am. Chem. Soc. 125 (50) (2003) 15589–15598.
[23] P.A. Rundquist et al., J. Chem. Phys. 91 (8) (1989) 4932–4941.
[24] R.J. Carlson, S.A. Asher, Appl. Spectrosc. 38 (3) (1984) 297–304.
[25] S.A. Asher, P.L. Flaugh, G. Washinger, Spectroscopy (Duluth, MN, U. S.) 1 (12) (1986) 26–31.
[26] S. Tandon, R. Kesavamoorthy, S.A. Asher, J. Chem. Phys. 109 (15) (1998) 6490–6496.
[27] P.A. Hiltner, I.M. Krieger, J. Phys. Chem. 73 (7) (1969) 2386–2389.
[28] I.M. Krieger, F.M. O'Neill, J. Am. Chem. Soc. 90 (12) (1968) 3114–3120.
[29] G. Pan, A.K. Sood, S.A. Asher, J. Appl. Phys. 84 (1) (1998) 83–86.
[30] L. Liu, P. Li, S.A. Asher, J. Am. Chem. Soc. 119 (11) (1997) 2729–2732.
[31] S.A. Asher et al., Phys. Rev. E: Stat., Nonlinear, Soft Matter Phys. 69 (6–2) (2004) 066619/1–066619/14.
[32] G. Pan, R. Kesavamoorthy, S.A. Asher, Phys. Rev. Lett. 78 (20) (1997) 3860–3863.
[33] J.M. Weissman et al., Science (Washington, DC) 274 (5289) (1996) 959–960.
[34] G. Pan et al., J. Am. Chem. Soc. 120 (26) (1998) 6518–6524.
[35] W. Wang, S.A. Asher, J. Am. Chem. Soc. 123 (50) (2001) 12528–12535.
[36] A. Tikhonov, R.D. Coalson, S.A. Asher, Phys. Rev. B: Condens. Matter Mater. Phys. 77 (23) (2008) 235404/1–235404/16.
[37] R. Biswas et al., Phys. Rev. B: Condens. Matter Mater. Phys. 57 (7) (1998) 3701–3705.

[38] A. Blanco et al., Nature (London) 405 (6785) (2000) 437–440.
[39] H. Miguez et al., Adv. Mater. (Weinheim, Ger.) 13 (21) (2001) 1634–1637.
[40] H.S. Sozuer, J.W. Haus, R. Inguva, Phys. Rev. B 45 (24) (1992) 13962.
[41] A. Moroz, C. Sommers, J. Phys. Condens. Matter 11 (4) (1999) 997–1008.
[42] K.P. Velikov, A. Moroz, A. van Blaaderen, Appl. Phys. Lett. 80 (1) (2002) 49–51.
[43] X. Jiang, T. Herricks, Y. Xia, Adv. Mater. (Weinheim, Ger.) 15 (14) (2003) 1205–1209.
[44] U. Jeong, Y. Xia, Adv. Mater. (Weinheim, Ger.) 17 (1) (2005) 102–106.
[45] U. Jeong et al., Nano Lett. 5 (5) (2005) 937–942.
[46] I.D. Hosein, C.M. Liddell, Langmuir 23 (5) (2007) 2892–2897.
[47] K.P. Velikov, A. van Blaaderen, Langmuir 17 (16) (2001) 4779–4786.
[48] T. Sugimoto, G.E. Dirige, A. Muramatsu, J. Colloid Interface Sci. 182 (2) (1996) 444–456.
[49] T. Sugimoto, S. Chen, A. Muramatsu, Colloids Surf., A 135 (1-3) (1998) 207–226.
[50] D.M. Wilhelmy, E. Matijevic, J. Chem. Soc., Faraday Trans. 1: Phys. Chem. Condens. Phases 80 (3) (1984) 563–570. 2 plates.
[51] T. Sugimoto, Chem. Eng. Technol. 26 (3) (2003) 313–321.
[52] T. Sugimoto, G.E. Dirige, A. Muramatsu, J. Colloid Interface Sci. 180 (1) (1996) 305–308.
[53] C. Joly-Duhamel, D. Hellio, M. Djabourov, Langmuir 18 (19) (2002) 7208–7217.
[54] P.M. Gilsenan, S.B. Ross-Murphy, Food Hydrocolloids 14 (3) (2000) 191–195.
[55] T. Sugimoto, Monodispersed Particles, first ed., Elsevier Science, Amsterdam, New York, 2001.
[56] H.G. Curme, C.C. Natale, J. Phys. Chem. 68 (10) (1964) 3009.
[57] K.A. Vaynberg, N.J. Wagner, R. Sharma, P. Martic, J. Colloid Interface Sci. 205 (1998) 131.
[58] P. Schindler, H.R. Kamber, Helv. Chim. Acta 51 (7) (1968) 1781.
[59] M.L. Hair, W. Hertl, J. Phys. Chem. 74 (1) (1970) 91.
[60] L.H. Allen, E. Matjevic, L. Meites, J. Inorg. Nucl. Chem. 33 (1971) 1293.
[61] J.P. Mercier, P. Morin, M. Dreux, A. Tambute, Chromatographia 48 (7/8) (1998) 529.
[62] P.L. Flaugh, S.E. O'Donnell, S.A. Asher, Appl. Spectrosc. 38 (6) (1984) 847–850.
[63] E.D. Palik, Handbook of Optical Constants of Solids, Academic Press, New York, 1998. pp. 597–619.
[64] J.W. Goodwin, R.H. Ottewill, A. Parentich, J. Phys. Chem. 84 (12) (1980) 1580–1586.
[65] A. Tikhonov, R.D. Coalson, S.A. Asher, Phys. Rev. B: Condens. Matter Mater. Phys. 77 (23) (2008) 235404/1–235404/16.
[66] P.D.T. Huibers, D.O. Shah, Langmuir 13 (22) (1997) 5995–5998.